



CrossMark
click for updates

Cite this: *RSC Adv.*, 2015, 5, 61710

Gold supported on Ti incorporated MCM-36 as efficient catalysts in propylene epoxidation with H₂ and O₂†

Fang Jin,^{ab} Tsung-Han Lin,^a Chih-Cheng Chang,^a Ben-Zu Wan,^c Jyh-Fu Lee^d and Soofin Cheng^{*a}

Novel catalysts consisting of gold nanoparticles (NPs) supported on the titanosilicate pillared MCM-36 (Si/Ti-MCM-36) with 2 nm mesopores were prepared. The influences of the Ti coordination environment on the particle size of the anchored Au NPs and their catalytic performances in propylene epoxidation with mixtures of H₂ and O₂ were investigated. The catalyst materials were characterized with Electron Probe Micro Analysis, X-ray diffraction, nitrogen sorption, UV-visible diffuse reflectance spectroscopy, transmission electron microscopy, and X-ray absorption spectroscopy. The coordination environment of Ti(IV) in Si/Ti-MCM-36 was found to be a mixture of octahedral (O_h) and tetrahedral (T_d). The Au loading was proportional to the amount of Ti incorporated in the porous silica. The higher loading of Ti in Si/Ti-MCM-36 anchored more Au and resulted in the formation of larger Au particles. The deposition-precipitation (DP) with NH₃ as a DP agent seemed to give Au NPs larger than those loaded by NaOH. The most efficient Au NPs size was about 1 nm, and Au NPs with sizes larger than 2 nm were not efficient for the propylene epoxide (PO) formation. By adjusting the Au and Ti synergy, the optimal PO formation rate over Au loaded Si/Ti-MCM-36 was 28.9 g_{PO} h⁻¹ g_{cat}⁻¹.

Received 9th May 2015
Accepted 8th July 2015

DOI: 10.1039/c5ra08621c

www.rsc.org/advances

1. Introduction

Propylene epoxide (PO) is a very important feed stock in chemical industry and widely used to produce a variety of derivatives such as polyurethane, propylene glycol, polyester resins and surfactants. The industrial PO production routes, such as chlorohydrins and organic peroxide processes, suffer from generating either environmentally unfriendly chlorinated compounds or co-products with lower demand and/or market values.¹ The direct epoxidation of propene with H₂O₂ over TS-1 catalyst and methanol as solvent is an alternative route in terms of greenness.¹ Nevertheless, the industrialization of hydrogen peroxide process suffers from some drawbacks, such as the expensive cost of the oxidant H₂O₂, difficulties in separating the azeotropic mixture of PO and methanol solvent, formation of the solvolysis side-products of glycol ethers as a result of the ring-opening

reaction of PO with methanol. Moreover, all the current processes require multiple reaction steps in the liquid phase. In 1998, Haruta and coworkers² discovered for the first time that propylene epoxidation could be achieved with hydrogen and oxygen on-site generating H₂O₂ over gold nanoparticles supported on TiO₂. Since then, the direct epoxidation of propylene to PO has gained considerable attention in the past sixteen years.

Various titanosilicates, including TiO₂/SiO₂,³ Ti-TUD,⁴ Ti-SBA-15,⁵ Ti-MCM-41,⁶ Ti-MCM-48,⁷ Ti-MWW,⁸ Ti-β,⁹ TS-2, TS-1,^{10,11} and alkaline treated TS-1 (ref. 12) have been investigated for propylene epoxidation. Sinha *et al.*¹³ claimed that the Ti incorporated oxide supports with high surface and mesopores were required to have well dispersed Au nanoparticles and give high yields of PO. Moreover, well-dispersed tetrahedral Ti sites in the silica supports and the size of the gold nanoparticles were considered to be the two important factors for an active catalyst. Although many studies have addressed the issue, the assignment of the gold active sites is still under debate. Gold nanoparticles with sizes in 2–5 nm were originally assigned as the active sites for the PO reaction in Au/TiO₂ and other Au/Ti-based oxides by Haruta's groups.^{2,14} Later, Haruta's groups proposed that the dominant gold active sites in Au/TS-1 for the PO reaction might be 55 gold atom clusters of ca. 1.4 nm diameter.¹⁵ Recently, Feng *et al.*¹⁶ identified the size-dependent activity of Au nanoparticles (2–5 nm) deposited on the exterior surface of TS-1 by employing uncalcined TS-1. The catalyst with Au nanoparticles about 2.5 nm was reported to have the best catalyst performance.

^aDepartment of Chemistry, National Taiwan University, Taipei 10617, Taiwan. E-mail: chem1031@ntu.edu.tw

^bKey Laboratory for Green Chemical Process of Ministry of Education, School of Chemical Engineering and Pharmacy, Wuhan Institute of Technology, Wuhan 430073, China

^cDepartment of Chemical Engineering, National Taiwan University, Taipei 10617, Taiwan

^dResearch Division, National Synchrotron Radiation Research Center, Hsinchu 300, Taiwan

† Electronic supplementary information (ESI) available. See DOI: 10.1039/c5ra08621c

MCM-22 zeolite (IZA code MWW) exhibits advantages of high flexibility in varying the pore structures by different post-treatments.¹⁷ The lamellar MWW structure comprises two independent 10-membered ring (MR) channels and 12-MR cups on the crystal exterior.¹⁷ Several of the MCM-22 derivatives were reported using the lamellar precursor, including delaminated MWW (ITQ-2), partially delaminated MWW (MCM-56) and the silica-pillared MWW (MCM-36).¹⁷ Recently, the relevant MWW-type zeolitic materials were comprehensively reviewed.^{17–19} Ti-incorporated MWW structures have attracted scientists because of their catalytic properties in partial oxidation reactions¹⁷ Wu *et al.*²⁰ and Fan *et al.*²¹ synthesized the titanosilicate zeolites, Ti-MWW and Ti-YNU-1, respectively, with 3D MWW micropore structures by using different reactive processes. Ti-YNU-1 has the same basic building unit as Ti-MWW but an expanded interlayer window from 10 to 12-MR and an enlarged 2.59 Å interlayer spacing.^{22,23} Recently, a new approach for preparing Ti incorporated MCM-36 material (Si/Ti-MCM-36) was developed in our laboratory by intercalating the MWW lamellar precursor with titanosilicate pillars.²⁴ Furthermore, when ERB-1, which was a borosilicate and aluminum-free analogue of MCM-22, was used instead of MCM-22 as the precursor, a more efficient pillared 2 nm mesopores and higher surface area were obtained. The material also exhibited better catalytic performance in liquid phase epoxidation of cyclohexene with *tert*-butyl hydroperoxide. This success encouraged us to investigate the performance of Au catalysts supported on the new type of Ti incorporated mesoporous MCM-36 in direct epoxidation of propylene with H₂ and O₂.

2. Experimental methods

2.1. Preparation of materials

The borosilicate of MWW structure, namely ERB-1 precursor or ERB-1(P), was prepared following the synthesis method reported by Millini *et al.*^{25,26} with the reactant ratio of Si : B : pyridine (PI) : H₂O = 1 : 0.75 : 1.4 : 19. The synthesis of Si/Ti-MCM-36 was started with a swelling step in a solution mixture of tetrapropylammonium hydroxide (TPAOH) and cetyltrimethylammonium bromide (CTMABr) with a relative weight ratio of TPAOH : CTMABr : H₂O = 1 : 4 : 330. The mixture sealed in a flask at 373 K for 16 h. The resulting swollen ERB-1 material was collected by filtration, washing with distilled water, and drying under vacuum. The swollen ERB-1 was then dispersed in a mixture of tetraethylorthosilicate (TEOS) and tetrabutylorthotitanate (TBOT) with TEOS/TBOT molar ratio varied in 40 : 1, 100 : 1, and 160 : 1, and the mixture was stirred at 353 K for 25 h. The material collected by filtration was dried at ambient condition. The hydrolyzation of TBOT and TEOS was carried out by suspending the dried solid in an aqueous solution at 313 K for 6 h at pH 9 adjusted with 1 M NH₃. Finally, the sample was calcinated at 723 K for 3 h in nitrogen and at 812 K for 6 h in air (heating rate of 2 K min⁻¹). The resultant materials were designated as xSi/Ti-MCM-36, where x is the Ti/Si molar ratio in the pillaring gel.

Gold was deposited on the supports by a deposition-precipitation (DP) method using sodium hydroxide or ammonia

as the base.^{27,28} Approximately, 0.1 g of HAuCl₄·3H₂O (Alfa Aesar, 99.99%) was dissolved in 25 mL of D.I. water stirring at 313 K, and the pH of the gold solution was adjusted with the base to 6. The neutralized gold solution was further stirred for 2 h at 313 K before 0.35 g of the support was added. The pH value of the solution was further adjusted to 7 with 0.1 M base in about 1 h, and the mixture was stirred for another 2 h at the same temperature and pH value. The solid was filtered, washed with 500 mL of D. I. H₂O, and dried under ambient condition for 12 h. The prepared gold catalysts were stored in sealed amber bottles at 277 K and used in 12 h for propene epoxidation reaction. The sample was designated *m*Au/*x*Si/Ti-MCM-36, where *m* represents the nominal number of wt% of gold in the DP solution *versus* the support. The *m* values of 1, 1.5, 3 and 4.5 correspond to the Au³⁺ precursor concentrations in the DP solution to be *ca.* 0.59, 1.1, 2.2, and 3.3 mM. The samples prepared with 0.1 M NH₃ as the base for controlling pH values are denoted as *m*AuNH₃/*x*Si/Ti-MCM-36, while others used NaOH as the base.

2.2. Characterization

X-ray powder diffraction patterns were recorded using a PANalytical X'Pert PRO diffractometer with a Cu-K_α radiation ($\lambda = 1.5418 \text{ \AA}$) operated at 40 mA and 45 kV. Diffuse reflectance (DR) UV-vis spectra were recorded using a Hitachi U-3310 spectrometer equipped with an integrating sphere detector, and BaSO₄ was the reference. The elemental analyses were determined using Electron Probe Micro Analysis (EPMA) in JEOL JXA-8200 Electron Probe. Transmission electron microscopy (TEM) photographs were obtained from a JEOL JEM-1200EX II Transmission Electron Microscope and Hitachi H-7100 Transmission Electron Microscope.

Au L_{III}-edge X-ray absorption spectra (XAS) were collected using the fluorescence mode at the beam lines 17C of the National Synchrotron Radiation Research Center (NSRRC) facility in Hsinchu, Taiwan. Standard operating condition was 1.5 GeV and 350 mA. The photon energy was guided using a fixed-exit double-crystal Si(111) monochromator and calibrated with a metallic Au foil (L_{III}-edge, 11 919 eV).

The X-ray absorption near-edge structure (XANES) and extended X-ray absorption fine structure (EXAFS) data were processed using the programs of IFEFFIT.²⁹ The EXAFS spectra with *k*³-weighted functions were fourier transformed (FT) over a photoelectron momentum (*k*) range of 2.5–12.1 Å⁻¹. Structural parameters were extracted from the first coordination shell, which was isolated by inverse transforming over a nonphase-corrected radial distance range (*r*-space) of 1.8–3.4 Å. The spectra were then fitted to the EXAFS equation.³⁰ The amplitude reduction factor (*S*₀²) value of 0.86 were determined from the reference standard (unirradiated Au foil) and kept constant for fitting all spectra. The interatomic distance *R*, the coordination number of first nearest neighbor (1NN), the difference of the Debye–Waller factor from the reference ($\Delta\sigma^2$), and the correction of the threshold energy (ΔE) were treated as free parameters during the fitting. Fitting analysis in both *k*¹- and *k*³-weighted fourier transforms was applied in order to obtain a unique set of

coordination number (CN) and $\Delta\sigma^2$ parameters. The photoelectron scattering-path amplitudes and phases were calculated by *ab initio* using FEFF8 (ref. 31) for a face-centered-cubic (fcc) structure of Au with a first nearest neighbor distance of 2.885 Å. The size dependent average CN of atoms in a 12-fold coordinated spherical particle can be estimated by $CN = 12(1 - 3/2D)R_{1NN}$, where R_{1NN} is the nearest neighbor distance and D is the average diameter of nanoparticles (NP).^{32–35}

2.3. Catalytic reaction

The catalytic performances of prepared catalysts were examined using a fixed bed flow system. The catalyst in powder form was packed in a quartz tubular microreactor (35 cm in length, inner diameter 6 mm, wall thickness 1.5 mm) equipped with an axial quartz thermocouple well (2 mm O.D.), which allowed monitoring of the temperature of catalyst bed. Typically, the epoxidation of propylene was carried out under atmosphere pressure, using 0.25 g of catalyst without dilution and a gas feed rate of 28 cm³ min⁻¹ in total, with a feed concentration of 10/10/10/70 vol% of He (99.9%), O₂ (99.9%), H₂ (99.9%), and C₃H₆ (99.8%). The corresponding space velocity was about 7000 cm³ h⁻¹ g_{cat}⁻¹. Before reaction, the catalyst was pretreated with a mixture of 10 vol% H₂ in He (28 cm³ min⁻¹) for 6 h, followed by 10 vol% O₂ in He (28 cm³ min⁻¹) at 523 K for 0.5 h, after that the temperature was set to 473 K under He flow and the reactants were introduced.

Reaction products were analyzed by an online gas chromatograph (Shimadzu GC-14B), containing a CP-wax 52CB and a Carboxen-1000 columns in two separate channels, with a flame ionization detector (FID) and a thermal conductivity detector (TCD), respectively. The CP-wax 52CB capillary column (0.53 mm × 50 m) was used to detect oxygenates (*i.e.*, acetaldehyde (AA), PO, acetone (ACE), propionaldehyde (PA), acrolein (ACR)), respectively, whereas the Carboxen-1000 column was used to analyze H₂, O₂, and CO₂ and propylene, respectively.

The propylene conversion, PO selectivity, H₂ conversion, and H₂ selectivity were defined as follows:

Propylene conversion ($X_{C_3H_6}$) = mol of (oxygenates + CO₂)/3/mol of propylene in feed.

Product selectivity (S_N) = mol of corresponding product/mol of (oxygenates + CO₂)/3,

where N is PO, or oxygenated side products, *i.e.*, AA, ACE, PA and ACR.

H₂ conversion (X_{H_2}) = mol of H₂ consumed/moles of H₂ in feed.

H₂ selectivity (S_{H_2}) = mol of PO formed/moles of H₂ consumed.

3. Results

3.1 Elemental analysis

The ERB-1 discovered by Bellussi *et al.* in 1988 (ref. 36) is actually an borosilicate isostructural with the MWW structure.

The EPMA analysis results in Table 1 show that all the pillared MCM-36 samples do not contain boron anymore. It has been confirmed that the swelling treatment of 3D-MWW precursor with TPAOH and CTMABr at elevated temperature and high pH value can leach nearly all the boron and also partially dissolve the framework silicon.^{24,37} The pillaring step with the mixture of TEOS and TBOT incorporated Ti in the MWW structure. Table 1 shows that the amount of incorporated Ti in Si/Ti-MCM-36 increases with decreasing the TEOS/TBOT ratio in the pillaring reagent, and the Si/Ti ratio decreases.

Table 1 also summarizes the Au loadings of the supported Au catalysts. For Au-loaded 100Si/Ti-MCM-36 samples, the actual Au loading is proportional to the concentration of the Au precursor used in DP solution. Au loading of 0.84 wt% was obtained with 3.3 mM Au³⁺ solution (4.5Au/100Si/Ti-MCM-36) and 0.12 wt% loading with 0.59 mM Au³⁺ solution (1Au/100Si/Ti-MCM-36).

When using identical concentrations of Au precursor for DP, the Au loading on *x*Si/Ti-MCM-36 was found to change with the Ti content in the support. The Au loading decreases slightly with the decrease of Ti content in Si/Ti-MCM-36. For example, the actual Au weight percentage loaded in the catalysts 40, 100 and 160Si/Ti-MCM-36 prepared with the same original 1.1 mM Au precursor concentrations decrease from 0.31, 0.19 to 0.14%. This is consistent with the results reported by other groups that higher Ti content leads to higher Au loading.^{8,38} The presence of Ti has been reported to be helpful in capturing the Au precursor during the DP process, which is originated from a certain affinity interaction between Ti species and Au precursor.¹³

In comparison of the DP agent for loading Au, NH₃ is more efficient to load Au on the supports than NaOH. When the same Au precursor concentration in the DP solution is used, 1.5Au/100Si/Ti-MCM-36 contains only 0.19 wt% Au, while 1.5AuNH₃/100Si/Ti-MCM-36, contains 0.74 wt% Au.

Table 1 The physico-chemical properties of the MCM-36 samples with different Si/Ti ratios

Sample	Si/Ti molar ^a	Si/B molar ^a	Au ^a loading (%) [wt%]
ERB-1	Na	57	—
40Si/Ti-MCM-36	15.3	∞	—
100Si/Ti-MCM-36	30	∞	—
160Si/Ti-MCM-36	94	∞	—
4.5Au/100Si/Ti-MCM-36 ^b	30	∞	0.84
3Au/100Si/Ti-MCM-36	30	∞	0.36
1.5Au/100Si/Ti-MCM-36	30	∞	0.19
1Au/100Si/Ti-MCM-36 ^b	30	∞	0.12
1.5Au/160Si/Ti-MCM-36 ^b	94	∞	0.14
1.5Au/40Si/Ti-MCM-36 ^b	15.3	∞	0.31
1.5AuNH ₃ /40Si/Ti-MCM-36	15.3	∞	1.1
1.5AuNH ₃ /100Si/Ti-MCM-36	30	∞	0.74
1.5AuNH ₃ /160Si/Ti-MCM-36	94	∞	0.38

^a Elemental analysis from EPMA. ^b Spent catalyst.

Basically, the relative Au amounts loaded in the final products can also be determined by the edge jump of an X-ray absorption spectrum collected in the transmission mode (like the XRF technique) in the linear range.^{39,40} However, the fluorescence mode can only give semiquantitative analysis results. The results shown in Fig. S1 (ESI[†]) obey the rule that the higher edge jumps of original XAS data correspond to higher Au contents in the catalysts, which confirms the EPMA results for the Au wt% contents.

3.2 X-ray diffraction

The small- and wide-angle XRD patterns of the samples are shown in Fig. 1(A) and (B), respectively. The ERB-1 precursor shows the diffraction (001) at about 3° which is attributed to the stacking of layered MWW structure along the *c*-direction with a distance of 27 Å. The Si/Ti-pillared MCM-36 samples show the (001) reflection shifts down to around 2°, corresponding to an increased *d*-spacing of 44 Å, and that implies mesopores of about 20 Å are generated by expanding the inter-layer space. Meanwhile, the (002) diffraction at 6.5° of the precursors almost disappears. These results are evidences for the successful expansion of the ERB-1 with the TEOS and TBOT mixture as the pillaring solvent. However, unlike the merging of (101) and (102) diffraction peaks for MCM-36 prepared from MCM-22 precursor reported in the literature,¹⁸ the Si/Ti-MCM-36 prepared from ERB-1(P) still exhibits two well resolved (101) and (102) diffractions peaks of ERB-1(P). That implies that a portion of the particles, probably the inner portion, may not be efficiently pillared.

The incorporation of Au did not significantly change the structure of Si/Ti-MCM-36 framework as shown in Fig. 2. However, for the samples with relatively larger Au loadings, diffraction peaks of Au metal appear at 38.2° and 44.4° in the XRD patterns, especially for the samples prepared with NH₃ as the DP agent, such as 4.5AuNH₃/40Si/Ti-MCM-36 and 4.5AuNH₃/100Si/Ti-MCM-36.

3.3 UV-vis diffuse reflectance spectroscopy

The Ti-incorporated supports with different Si/Ti ratios were examined with DR UV-vis analysis in order to understand the

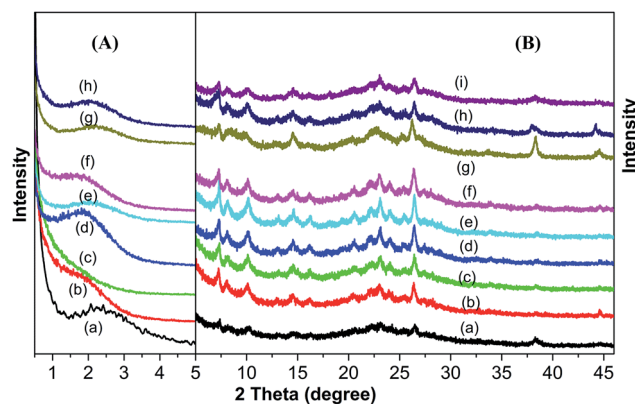


Fig. 2 (A) Small angle and (B) wide angle XRD patterns of (a) 4.5Au/100Si/Ti-MCM-36, (b) 3Au/100Si/Ti-MCM-36, (c) 1.5Au/100Si/Ti-MCM-36, (d) 1Au/100Si/Ti-MCM-36, (e) 1.5Au/160Si/Ti-MCM-36, (f) 1.5Au/40Si/Ti-MCM-36, (g) 1.5AuNH₃/40Si/Ti-MCM-36, (h) 1.5AuNH₃/100Si/Ti-MCM-36, and (i) 1.5AuNH₃/160Si/Ti-MCM-36.

coordination geometry of the Ti(IV) cations. The spectra of Si/Ti-MCM-36 materials are shown in Fig. 3. All the samples have two peaks at 220 and 260 nm. However, the intensity of ~260 nm peak obviously decreases with the decrease of Ti loading. According to Chen *et al.*,⁴¹ the 220 nm band is assigned to charge transfer from O²⁻ to Ti⁴⁺ of the tetrahedral (*T_d*) coordination, while the 260 nm band is attributed to charge transfer from O²⁻ to Ti⁴⁺ in octahedral (*O_h*) coordination. Therefore, the incorporated Ti is more favorable to be present in *T_d* coordination state than *O_h* state when Ti loading is low or the Si/Ti ratio is high. In other words, Ti is highly dispersed in the silica matrix when Ti loading is low. In contrast, titanium oxide clusters would form when the Ti loading increases.

After supporting Au on Si/Ti-MCM-36 by the DP method, the materials have the color of white. However, the used catalysts after PO synthesis reaction display different colors, such as blue, pink and brown, and it is a result of the presence of Au nanoparticles (NPs) of different amounts and particles sizes. These results indicate that Au was reduced to metallic state during the

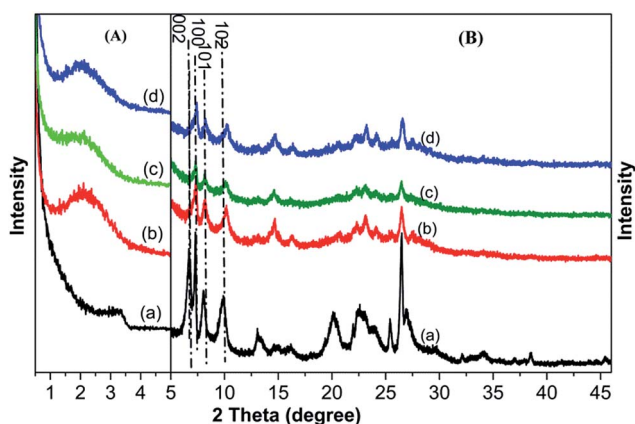


Fig. 1 (A) Small angle and (B) wide angle XRD patterns of (a) ERB-1(P), (b) 40Si/Ti-MCM-36, (c) 100Si/Ti-MCM-36, (d) 160Si/Ti-MCM-36.

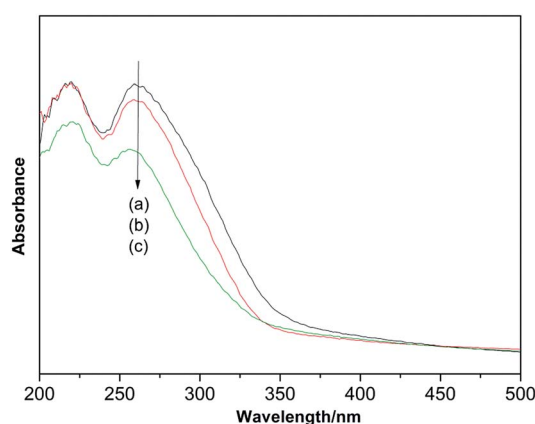


Fig. 3 DR UV-vis spectra of (a) 40Si/Ti-MCM-36, (b) 100Si/Ti-MCM-36 and (c) 160Si/Ti-MCM-36.

catalytic reaction, although it was originally deposited on the supports in the hydroxide or oxide form. Their UV-vis spectra exhibit a characteristic absorption band in the visible region around 500–600 nm as shown in Fig. 4. The samples with larger amounts of the Au loadings, such as the 1.5Au/100Si/Ti-MCM-36, 1.5AuNH₃/40Si/Ti-MCM-36, 1.5AuNH₃/100Si/Ti-MCM-36, 1.5AuNH₃/160Si/Ti-MCM-36 and 1.5AuNH₃/160Si/Ti-MCM-36 have an obvious absorption band. This absorption band was due to surface plasmon vibrations of gold, and the wavenumbers are dependent on the gold particle size.⁴² The peak has red shift with the increase of the NPs size. Fig. 4 also shows that the wavelength of this Au plasmon UV-vis peak for 4.5Au/100Si/Ti-MCM-36 is slightly lower than those of 1.5AuNH₃/40Si/Ti-MCM-36 and 1.5AuNH₃/100Si/Ti-MCM-36, although they have similar Au loadings. On the other hand, the peak position is almost the same as that of 1.5AuNH₃/160Si/Ti-MCM-36, which contains more than twice amount of Au. This is evidence that the Au NPs loaded by using NH₃ as the DP agent would give larger Au NPs than those prepared with NaOH.

3.4 Au L_{III}-edge XAS spectroscopy

EXAFS analysis of the Au L_{III}-edge XAS spectra of spent catalysts was carried out to determine the CNs of Au atoms and thus to calculate the sizes of the Au NPs. The Fourier transforms (FT) of Au L_{III}-edge k^3 -weighted EXAFS spectra of the catalysts Au/ x Si/Ti-MCM-36 are shown in Fig. 5, and the k^3 -weighted EXAFS spectra and the curve fitting results are summarized in Fig. S2 and S3 (ESI[†]). These results are compared with the spectrum of the Au foil. The refined fitting parameters are given in Table 2. From the obtained coordination number, a mean Au particle size was calculated by assuming Au metal in spherical particles

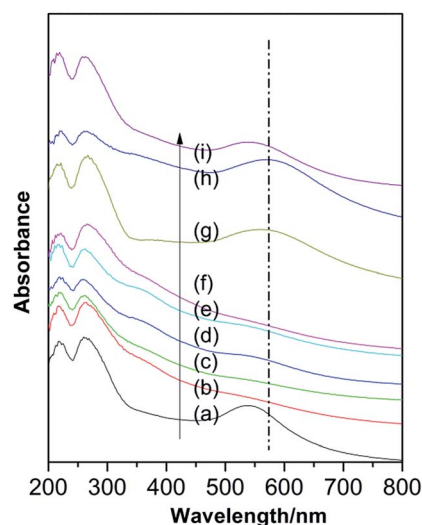


Fig. 4 DR UV-vis spectra of (a) 4.5Au/100Si/Ti-MCM-36, (b) 3Au/100Si/Ti-MCM-36, (c) 1.5Au/100Si/Ti-MCM-36, (d) 1Au/100Si/Ti-MCM-36, (e) 1.5Au/160Si/Ti-MCM-36, (f) 1.5Au/40Si/Ti-MCM-36, (g) 1.5AuNH₃/40Si/Ti-MCM-36, (h) 1.5AuNH₃/100Si/Ti-MCM-36 and (i) 1.5AuNH₃/160Si/Ti-MCM-36.

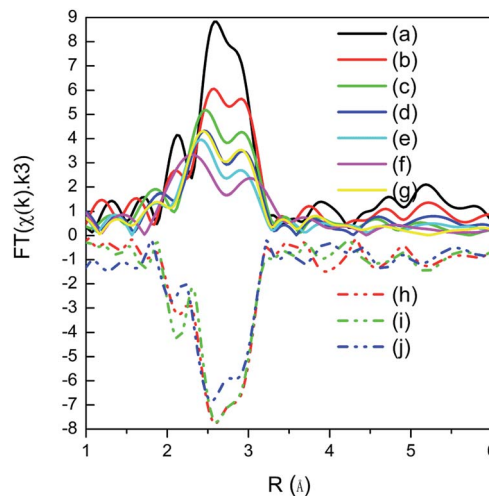


Fig. 5 EXAFS of the Au L_{III}-edge phase-uncorrected Fourier transform spectra of the $\chi(k) \times k^3$ weighted in R space after applying a window around the first shell from 1.6–3.6 Å. (a) Gold foil, (b) 4.5Au/100Si/Ti-MCM-36, (c) 3Au/100Si/Ti-MCM-36, (d) 1.5Au/100Si/Ti-MCM-36, (e) 1Au/100Si/Ti-MCM-36, (f) 1.5Au/160Si/Ti-MCM-36, (g) 1.5Au/40Si/Ti-MCM-36, (h) 1.5AuNH₃/40Si/Ti-MCM-36 (vertical value multiple -1), (i) 1.5AuNH₃/100Si/Ti-MCM-36 (vertical value multiple -1), (j) 1.5AuNH₃/160Si/Ti-MCM-36 (vertical value multiple -1).

and fcc structure.^{5,43} The resulting mean particle sizes of Au on the samples are also listed in Table 2.

The spectra and calculated results of 100Si/Ti-MCM-36 loaded with different amounts of Au varied from 0.84 to 0.36 wt% show that smaller Au NPs are generated when less amounts of Au are loaded on the support, and concomitantly the lower average coordination numbers are obtained for Au atoms. It is also noticed that the first shell near-neighbor distance, R , decreases slightly with lower Au loading, in consistent with the literature report.⁵ Furthermore, the Au NPs size has little variation with the Au loadings lower than 0.36 wt%.

In comparison of the catalysts with different Ti-contents, *i.e.*, 1.5Au/ x Si/Ti-MCM-36, the correlations between Au NPs sizes and Au loadings are similar. The Au NPs sizes increase with increasing the Ti content. As to the samples prepared using NH₃ as DP agent, relatively larger gold particles are formed, in agreement with the results from the UV-vis spectra.

3.5 Transmission electron microscopy

Fig. S4 (ESI[†]) shows the TEM images of two series of samples, namely Au supported on Si/Ti-MCM-36 prepared by NaOH and NH₃ as the neutralization agents with different Ti contents. The size distribution of the gold NPs analyzed by Digital Micrograph Demo software are shown in Fig. 6. Fig. 6(a)–(c) compare the samples with gold loadings of nominal 1.5 wt% with NaOH as neutralization agent over the x Si/Ti-MCM-36. The average sizes of gold NPs are about 2.0 nm, 1.5 nm, and 1.2 nm for $x = 40, 100, 160$, respectively. The effect of neutralization agents in DP method on the gold NPs size distributions is shown in Fig. 6(a)–(c) versus Fig. 6(d)–(f). The

Table 2 Refined fitting parameters from Au L_{III}-edge EXAFS analysis of the first coordination shell for different supported Au samples in comparison with that of Au foil as the reference material^a

Sample	Ave. CN	R (Å)	S ₀ ² (set)	Δσ ² (Å ²)	ΔE (eV)	Estimated Au NPs size (nm)
Gold foil	12.0	2.86	0.86	0.01	4.62	—
4.5Au/100Si/Ti-MCM-36	9.9	2.86	0.86	0.01	5.99	2.43
3Au/100Si/Ti-MCM-36	8.6	2.84	0.86	0.01	5.30	1.49
1.5Au/100Si/Ti-MCM-36	7.9	2.82	0.86	0.01	4.72	1.25
1Au/100Si/Ti-MCM-36	7.9	2.82	0.86	0.01	4.59	1.23
1.5Au/160Si/Ti-MCM-36	6.9	2.82	0.86	0.01	5.28	0.99
1.5Au/40Si/Ti-MCM-36	8.9	2.84	0.86	0.01	5.54	1.67
1.5AuNH ₃ /40Si/Ti-MCM-36	11.2	2.85	0.86	0.01	5.04	6.34
1.5AuNH ₃ /100Si/Ti-MCM-36	10.8	2.85	0.86	0.01	5.21	4.24
1.5AuNH ₃ /160Si/Ti-MCM-36	9.8	2.85	0.86	0.01	4.08	2.34

^a CN, R, S₀², σ² and ΔE are the coordination number, Au–Au bond distance, amplitude reduction factor, Debye–Waller factor and energy correction number, respectively.

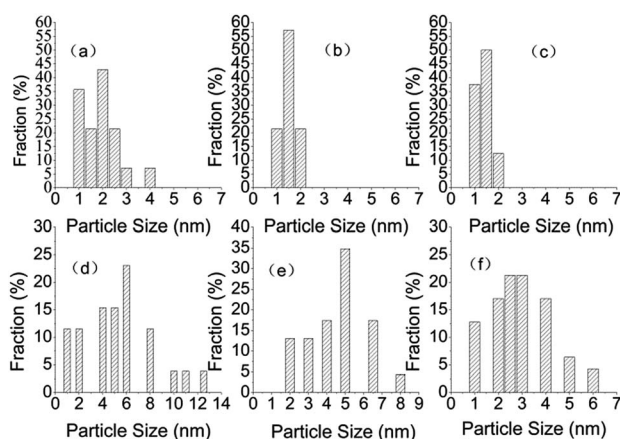


Fig. 6 The size distributions of gold nanoparticles of (a) 1.5Au/40Si/Ti-MCM-36, (b) 1.5Au/100Si/Ti-MCM-36, (c) 1.5Au/160Si/Ti-MCM-36, (d) 1.5AuNH₃/40Si/Ti-MCM-36, (e) 1.5AuNH₃/100Si/Ti-MCM-36, (f) 1.5AuNH₃/160Si/Ti-MCM-36.

gold NPs prepared with NH₃ as the neutralization agent are apparently larger and have wider distribution than those prepared with NaOH agent.

3.6 Catalytic performance

The Au/xSi/Ti-MCM-36 catalysts were applied for the direct propene epoxidation with O₂ and H₂ in a plug-flow system for about 6 h. The catalytic activities at time on stream (TOS) of 10 min and the average in 6 h are summarized in Table 3 and the completed data are shown in Table S1 (ESI[†]). The catalytic activities are expressed in terms of propene conversion ($X_{C_3H_6}$), PO selectivity (S_{PO}) and side products selectivities, PO yield, hydrogen conversion (X_{H_2}), and hydrogen selectivity (S_{H_2}). S_{H_2} is defined by moles of PO/moles of H₂ consumed, which is to differentiate the efficiency of H₂ consumed for propylene epoxidation from that consumed in the side reactions, such as direct reaction with O₂ for H₂O production or hydrogenation of propylene to form propane. Two PO formation rates are

shown. One is the specific rate or yield per hour based on per kg of catalyst and are called PO formation rate. The other PO rate is turnover frequency (TOF) based on per gram of gold, and that can demonstrate the Au efficiency.³

Over the 100Si/Ti-MCM-36 supported Au catalysts, the four catalysts with similar Au NPs sizes but the decrease of Au loadings from 2 wt% to 1 wt%, the $X_{C_3H_6}$ decreases and S_{PO} increases at the same time. The maximum Au efficiency and S_{H_2} reach 14.6 g_{PO} h⁻¹ g_{Au}⁻¹ and 9.7% over 1.5Au/100Si/Ti-MCM-36 catalyst, and the PO formation rate over this catalyst (27.7 g_{PO} h⁻¹ kg_{cat}⁻¹) is close to that over 3Au/100Si/Ti-MCM-36 (28.9 g_{PO} h⁻¹ kg_{cat}⁻¹). It also shows that the catalysts with the lower Au loadings have lower stability during the reaction, when comparing the catalytic activities at beginning and after 6 h reaction. Furthermore, when Au loadings are higher than 3.8 wt%, the Au/100Si/Ti-MCM-36 catalyst exhibits the worst catalytic performance, namely 50% selectivity of CO₂, a high H₂ conversion (about 33%) with mostly generating H₂O and producing only 3.8% PO (Table S1[†]). This phenomenon is explained by its much too large Au NPs size than others.

Although both series of the catalysts 1.5Au/xSi/Ti-MCM-36 exhibit similar tendency that the actual Au content and the corresponding NPs size increase with the Ti content, their catalytic performance trends are different. The optimum catalytic activity was found for 1.5Au/xSi/Ti-MCM-36 with nominal Si/Ti ratio of 100 in terms of the PO formation rate, Au efficiency, S_{PO} and S_{H_2} .

The phenomena were observed on 1.5AuNH₃/xSi/Ti-MCM-36 series that by using NH₃ instead of NaOH as the DP neutralization agent, the PO yields decrease significantly while the propanal (PA) selectivities increase dramatically.

In the reaction temperatures of 433–498 K, it is found that the $X_{C_3H_6}$ and X_{H_2} increase but S_{PO} and S_{H_2} decrease with increasing the reaction temperature over almost all the catalysts. Moreover, based on the PO formation rate the best reaction temperature is 453 K over Si/Ti-MCM-36 supported Au catalysts.

Table 3 Catalytic performance of Si/Ti-MCM-36 supported Au catalysts in propene epoxidation with H₂ and O₂^a

Catalyst	Si/Ti atomic ratio	Au wt%	T (K)	PO yield (%)	Propene conv. (%)	Selectivity ^b (%)			
						PO	PA	ACR	ACE
4.5Au/100Si/Ti-MCM-36	30	0.84	453	(0.9)	(0.88)	(84.93)	(0)	(4.55)	(0)
				0.67	0.71	93.02	0	0.91	0
				0.51	0.55	94.49	0	1.14	0
3Au/100Si/Ti-MCM-36	30	0.36	453	(1.88)	(2.98)	(62.99)	(1.68)	(4.7)	(0.34)
				1.01	1.57	63.08	0	14.68	0
				0.97	1.2	81.07	0	8.25	0
1.5Au/100Si/Ti-MCM-36	30	0.19	453	(1.8)	(2.19)	(82.24)	(1.37)	(0)	(0)
				1.39	1.61	86.61	0.23	0	0
				1.33	1.49	90.74	0.3	0	0
1Au/100Si/Ti-MCM-36	30	0.12	453	(0.93)	(1.08)	(86.02)	(0)	(0)	(0)
				0.48	0.61	77.49	0	0	0
				1.31	(2.12)	(61.83)	(5.19)	(2.83)	(0)
1.5Au/40Si/Ti-MCM-36	15.3	0.31	453	0.39	0.65	62.9	9.18	0.57	0
				0.39	0.97	41.39	5.69	0	0
				0.37	0.84	57.02	4.62	0	0
1.5AuNH ₃ /40Si/Ti-MCM-36	15.3	1.1	453	(0.18)	(2.31)	(7.99)	(87.88)	(0)	(0)
				0.29	1.63	16.81	68.48	0	0
				0.36	2.13	16.82	80.86	0	0
1.5AuNH ₃ /100Si/Ti-MCM-36	30	0.74	453	(0.43)	(2.32)	(18.7)	(79.31)	(0)	(0)
				0.36	2.13	16.82	80.86	0	0
				0.19	0.59	31.39	56.48	0	0
1.5AuNH ₃ /160Si/Ti-MCM-36	94	0.38	453	(0.04)	(0.49)	(8.5)	(73.47)	(0)	(0)
				0.19	0.59	31.39	56.48	0	0
				0.19	0.59	31.39	56.48	0	0

^a Reaction condition: 0.25 g catalysts, 433–498 K, space velocity: 7000 mL min⁻¹ g_{cat}⁻¹. ^b PO: propylene oxide, PA: propanal, ACR: acrolein, ACE: acetone. The catalytic performance data in the bracket is collect after 10 min reaction; the other data is from the average of 6 h reaction.

4. Discussion

4.1 Effect of Au particle size on PO synthesis

The Au particle sizes estimated from the 1NN coordination numbers of Au L_{III}-edge EXAFS suggest that the average Au particles are ranged from 1 to 6 nm, which are slightly lower than the average sizes determined from TEM images. It has been reported that the Au NPs with size smaller than 1 nm are invisible in the TEM images.^{11,15,27} In comparison, EXAFS is a more sensitive technique to determine the average size of poly-dispersed Au particles, especially toward diameter smaller than 1 nm.⁴ Nevertheless, there are correlations between the TEM and EXAFS results of Au particle sizes, despite of the higher sensitivity of EXFAS technique towards smaller particles.

The Au NPs size is considered to be one of the critical factors to influence the catalytic performance in propylene oxidation.⁴ Gold is believed to firstly catalyze the reaction of O₂/H₂ to form hydrogen peroxide, which then migrates to Ti(IV) sites on the supports to form titanium hydroperoxide species, and the latter react with propylene to form epoxide.^{2,3,44–46} The Au catalysts prepared using NH₃ as the neutralization agent have much higher Au loadings and larger NPs sizes than the corresponding samples with NaOH as neutralization agent over both Si/Ti-MCM-36 supports, as depicted from the EPMA, XRD, UV-vis and EXAFS analysis results. All the catalysts with Au NPs sizes larger than 2 nm have very low PO yields, as depicted in Table

S1.† Moreover, PA was found to be the principal product obtained besides propylene oxide over these catalysts. For the catalysts with different Au loadings but same supports, the overloaded Au on the supports 100Si/Ti-MCM-36 causes the formation of larger Au NPs (more than 2 nm), which are not efficient for the PO formation. This observation is in consistency with the literature reports.^{13,47} Possible explanation is that the formed hydrogen peroxide is more difficult to migrate to Ti sites on the larger Au particles because of longer distance and less interfacial area between gold particles and the supports. Instead, hydrogen peroxide is decomposed to H₂O or involved in nonselective oxidation.

4.2 Effect of Ti coordination environment on PO synthesis

For 1.5Au/xSi/Ti-MCM-36 catalysts, the actual Au loading and the corresponding Au NPs size increase with the Ti content in the supports. It is widely accepted that the higher Ti contents in Si/Ti-MCM-36 can anchor more Au and result in the formation of larger particles. The most active catalyst 1.5Au/100Si/Ti-MCM-36 has Au NPs size of about 1.25 nm, which is in between 0.99 nm of 1.5Au/160Si/Ti-MCM-36 and 1.66 nm of 1.5Au/40Si/Ti-MCM-36. According to literature,^{48–50} it is interesting to find that the Au NPs are larger in size when Ti in the supports coexisted in O_h and T_d coordinations, most of which is incorporated in the mesopores by grafting method. In contrast, the active Au NPs are smaller in the supports containing

absolutely isolated T_d Ti, which are almost prepared by the hydrothermal synthesis. These results are in consistence with our observation that the Au NPs supported on Si/Ti-MCM-36 with higher contents of O_h coordinated Ti is a little larger than that of lower contents of O_h coordinated Ti on the support.

The coordination environment of incorporated Ti in the supports has great influence on the loading and particle size of the anchored Au, as well as its catalytic performance. The optimal reaction temperature of Au/xSi/Ti-MCM-36 catalysts is evidence for the influence of Ti species in the supports on the catalytic performance. The change in catalytic temperature of Au on different supports for PO formation was reported in the literature.¹ The propylene epoxidation reaction should be carried out at temperatures below 373 K over the Au/TiO₂ catalysts, because PO is favorable to further oxidization to ACR, CO₂ and H₂O at higher temperatures. However, when replacing TiO₂ with highly dispersed TiO₂ on SiO₂ surfaces or TS-1, the operating temperature could be raised to 423–473 K.¹ Therefore, the optimal reaction temperature 453 K of Au/xSi/Ti-MCM-36 indicates that the Ti species is well dispersed in the supports. The most active Au NPs size of about 1.25 nm for the catalysts 1.5Au/xSi/Ti-MCM-36 is in consistent with the active Au particle size range for the catalysts with Ti in the supports coexisted in O_h and T_d coordinations.^{4,5,50}

4.3 The synergy of Au and Ti for PO formation

It has been reported that the epoxidation occurs at or close to the interface of Au–Ti sites.⁴ A good synergy between gold and titanium could limit water formation which occurs on the gold sites not adjacent to titanium.^{3,8} The Au loadings in xAu/100Si/Ti-MCM-36 samples with fixed Ti content but Au precursor concentrations varied in 1, 1.5 and 3 wt% have similar sizes of Au NPs (1.2–1.5 nm). The variation in catalytic activities of these three catalysts may demonstrate the synergy effect. The highest Au efficiency and S_{H_2} are observed on 1.5Au/100Si/Ti-MCM-36 (Table S1†), which should reach the best synergy between Au and Ti. Doubling the actual Au loading on 3Au/100Si/Ti-MCM-36 increases the $X_{C_3H_6}$ and X_{H_2} . However, the insufficient Ti content causes the insufficient hydroperoxy intermediates formed at the Ti sites for the PO formation. Instead, the redundant C₃H₆ combustion occurs on the Au surfaces,¹³ and CO₂ and H₂O are formed.³ It is evidenced by the increased S_{CO_2} and decreased S_{H_2} in comparison of 3Au/100Si/Ti-MCM-36 with 1.5Au/100Si/Ti-MCM-36. On the other hand, the decrease of Au loading from 1.5 to 1 wt% causes faster deactivation of the catalyst, which is attributed to that insufficient hydrogen peroxide is formed on Au NPs, and excessive Ti may inhibit the desorption of formed PO from the supports and deactivate the catalyst.⁸

5. Conclusions

Started from the ERB-1 precursor, the Ti incorporated expanded MWW layers of mesoporous Si/Ti-MCM-36 materials were synthesized as the supports for the Au catalysts. The Au

nanoparticles loaded on these supports by DP method were capable to catalyze gas-phase propylene epoxidation with H₂ and O₂.

The small and wide angle XRD studies confirmed the expanded structure between the layers and the reservation of the internal MWW zeolitic structure after incorporation of Ti and Au. After Au loading by DP method the mesopores of Si/Ti-MCM-36 were still preserved. The UV-vis spectra and EPMA analyses indicated that the Ti loading and ratio of O_h/T_d coordinated Ti in Si/Ti-MCM-36 could be controlled by adjusting the ratio of TEOS/TBOT precursors in the pillaring solvent.

The support plays important roles in affecting the Au loading and NPs sizes. The Au NPs loaded by NH₃ as DP agent were larger than those loaded by NaOH. On the other hand, the loading and size of gold particles had direct correlation with Ti contents on both series of Si/Ti-MCM-36 catalysts. Moreover, less amounts of Au and smaller NPs were loaded on Si/Ti-MCM-36 with lower content of Ti.

The catalytic performances of Au loaded Si/Ti-MCM-36 in propylene epoxidation proved that the Au NPs with particle size larger than 2 nm were not efficient for the PO formation and PA was the principal product. The most efficient catalysts contained Au NPs of about 1 nm. The synergy of Au and Ti was found important for PO formation. Overloading Au could result in the redundant C₃H₆ combustion and reduction of the H₂ selectivity to PO. Nevertheless, the insufficient Au loading could not generate enough H₂O₂ for the PO formation and excessive Ti would inhibit desorption of formed PO from the supports and cause catalyst deactivation. The optimal reaction temperature for Au/Si/Ti-MCM-36 is 453 K.

Acknowledgements

The financial supports from Ministry of Science & Technology, Taiwan (NSC101-2113-M-002-012-MY3, NSC102-2811-M-002-136) is gratefully acknowledged. F. Jin also acknowledges the supports of Natural Science Foundation, China (NSFC 21306143) and Scientific Research Foundation for the Returned Overseas Chinese Scholars, Education Ministry, China. Acknowledgement is also extended to Prof. H.C. Lin and Mr. C.Y. Kao, Ms. Y.Y. Yang and C.-Y. Chien of Instrumentation Center, National Taiwan University for the assistances in EPMA and EM experiments.

References

- 1 H. Masatake and K. Jun, in *Mechanisms in Homogeneous and Heterogeneous Epoxidation Catalysis*, ed. S. T. Oyama, Elsevier B.V., Netherland, 2008.
- 2 T. Hayashi, K. Tanaka and M. Haruta, *J. Catal.*, 1998, **178**, 566.
- 3 J. Chen, S. J. A. Halin, E. A. Pidko, M. W. G. M. Verhoeven, D. M. P. Ferrandez, E. J. M. Hensen, J. C. Schouten and T. A. Nijhuis, *ChemCatChem*, 2013, **5**, 467.
- 4 J. Lu, X. Zhang, J. J. Bravo-Suárez, K. K. Bando, T. Fujitani and S. T. Oyama, *J. Catal.*, 2007, **250**, 350.

- 5 E. Sacaliuc, A. M. Beale, B. M. Weckhuysen and T. A. Nijhuis, *J. Catal.*, 2007, **248**, 235.
- 6 A. K. Sinha, S. Seelan, T. Akita, S. M. Tsubota and M. Haruta, *Appl. Catal., A*, 2003, **240**, 243.
- 7 B. S. Uphade, T. Akita, T. Nakamura and M. Haruta, *J. Catal.*, 2002, **209**, 331.
- 8 Y. Ren, L. Xu, L. Zhang, J. Wang, Y. Liu, M. He and P. Wu, *Pure Appl. Chem.*, 2012, **84**, 561.
- 9 M. Haruta, B. S. Uphade, S. Tsubota and A. Miyamoto, *Res. Chem. Intermed.*, 1998, **24**, 329.
- 10 W.-S. Lee, M. Cem Akatay, E. A. Stach, F. H. Ribeiro and W. Nicholas Delgass, *J. Catal.*, 2013, **308**, 98.
- 11 W.-S. Lee, M. Cem Akatay, E. A. Stach, F. H. Ribeiro and W. N. Delgass, *J. Catal.*, 2014, **313**, 104.
- 12 J. Huang, T. Takei, T. Akita, H. Ohashi and M. Haruta, *Appl. Catal., B*, 2010, **95**, 430.
- 13 A. K. Sinha, S. Seelan, S. Tsubota and M. Haruta, *Top. Catal.*, 2004, **29**, 95.
- 14 C. Qi, J. Huang, S. Bao, H. Su, T. Akita and M. Haruta, *J. Catal.*, 2011, **281**, 12.
- 15 J. Huang, E. Lima, T. Akit, A. Guzmán, C. Qi, T. Takei and M. Haruta, *J. Catal.*, 2011, **278**, 8.
- 16 X. Feng, X. Duan, G. Qian, X. Zhou, D. Chen and W. Yuan, *J. Catal.*, 2014, **317**, 99.
- 17 U. Díaz, *Chem. Eng.*, 2012, **2012**, 1.
- 18 W. J. Roth and D. L. Dorset, *Microporous Mesoporous Mater.*, 2011, **142**, 32.
- 19 W. J. Roth, in *Stud. Surf. Sci. Catal.*, ed. H. V. B. A. C. Jíří Čejka and S. Ferdi, Elsevier, 2007, p. 221.
- 20 P. Wu, T. Tatsumi, T. Komatsu and T. Yashima, *Chem. Lett.*, 2000, **29**, 774.
- 21 W. B. Fan, P. Wu, S. Namba and T. Tatsumi, *Angew. Chem., Int. Ed.*, 2004, **43**, 236.
- 22 J. F. Ruan, P. Wu, B. Slater and O. Terasaki, *Angew. Chem., Int. Ed.*, 2005, **44**, 6719.
- 23 L. L. Wang, Y. M. Liu, Y. Wang, W. Xie, M. Y. He and P. Wu, *Stud. Surf. Sci. Catal.*, 2008, **174**, 24.
- 24 F. Jin, C.-C. Chang, C.-W. Yang, J.-F. Lee, L.-Y. Jang and S. Cheng, *J. Mater. Chem. A*, 2015, **3**, 8715.
- 25 R. Millini, G. Perego, W. O. Parker Jr, G. Bellussi and L. Carluccio, *Microporous Mesoporous Mater.*, 1995, **4**, 221.
- 26 P. Wu, T. Tatsumi, T. Komatsu and T. Yashima, *J. Phys. Chem. B*, 2001, **105**, 2897.
- 27 W.-S. Lee, L.-C. Lai, M. Cem Akatay, E. A. Stach, F. H. Ribeiro and W. N. Delgass, *J. Catal.*, 2012, **296**, 31.
- 28 F. Moreau, G. C. Bond and A. O. Taylor, *Chem. Commun.*, 2004, 1642.
- 29 B. Ravel and M. Newville, *J. Synchrotron Radiat.*, 2005, **12**, 537.
- 30 E. A. Stern, *Phys. Rev. B: Solid State*, 1974, **10**, 3027.
- 31 A. L. Ankudinov, B. Ravel, J. J. Rehr and S. D. Conradson, *Phys. Rev. B: Condens. Matter Mater. Phys.*, 1998, **58**, 7565.
- 32 S. de Panfilis, F. d'Acapito, V. Haas, H. Konrad, J. Weissmüller and F. Boscherini, *Phys. Lett. A*, 1995, **207**, 397.
- 33 A. I. Frenkel, C. W. Hills and R. G. Nuzzo, *J. Phys. Chem. B*, 2001, **105**, 12689.
- 34 A. Jentys, *Phys. Chem. Chem. Phys.*, 1999, **1**, 4059.
- 35 I. Anatoly, A. Y. Frenkel, C. Chana and V. Relja, *Annu. Rev. Anal. Chem.*, 2011, **4**, 23.
- 36 G. Bellussi, G. Perego, M. G. Clerici and A. Giusti, EP293032, 1988.
- 37 S. Maheshwari, E. Jordan, S. Kumar, F. S. Bates, R. L. Penn, D. F. Shantz and M. Tsapatsis, *J. Am. Chem. Soc.*, 2008, **130**, 1507.
- 38 J. Lu, X. Zhang, J. J. Bravo-Suárez, T. Fujitani and S. T. Oyama, *Catal. Today*, 2009, **147**, 186.
- 39 H. Y. Lee, T. B. Wu and J. F. Lee, *J. Appl. Phys.*, 1996, **80**, 2175.
- 40 H. Wang, F. Casper, T. Gasi, V. Ksenofontov, B. Balke, G. H. Fecher, C. Felser, Y.-K. Hwu and J.-J. Lee, *J. Phys. D: Appl. Phys.*, 2012, **45**, 295001.
- 41 S.-Y. Chen, C.-Y. Tang, J.-F. Lee, L.-Y. Jang, T. Tatsumi and S. Cheng, *J. Mater. Chem.*, 2011, **21**, 2255.
- 42 J. C. Martínez, N. A. Chequer, J. L. González and T. Cordova, *Nanosci. Nanotechnol.*, 2012, **2**, 184.
- 43 F. Farges, G. E. Brown Jr and J. J. Rehr, *Phys. Rev. B: Condens. Matter Mater. Phys.*, 1997, **56**, 1809.
- 44 T. A. Nijhuis, T. Visser and B. M. Weckhuysen, *J. Phys. Chem. B*, 2005, **109**, 19309.
- 45 L. Cumarantunge and W. N. Delgass, *J. Catal.*, 2005, **232**, 38.
- 46 W.-S. Lee, M. Cem Akatay, E. A. Stach, F. H. Ribeiro and W. Nicholas Delgass, *J. Catal.*, 2012, **287**, 178.
- 47 B. Taylor, J. Lauterbach and W. N. Delgass, *Appl. Catal., A*, 2005, **291**, 188.
- 48 B. Chowdhury, J. J. Bravo-Suárez, M. Daté, S. Tsubota and M. Haruta, *Angew. Chem., Int. Ed.*, 2006, **45**, 412.
- 49 T. A. Nijhuis, E. Sacaliuc-Parvulescu, N. S. Govender, J. C. Schouten and B. M. Weckhuysen, *J. Catal.*, 2009, **265**, 161.
- 50 C.-H. Liu, Y. Guan, E. J. M. Hensen, J.-F. Lee and C. M. Yang, *J. Catal.*, 2011, **282**, 94.